ACS Catalysis

Research Article

pubs.acs.org/acscatalysis

Electrocatalytic Enhancement of Salicylic Acid Oxidation at Electrochemically Reduced TiO_2 Nanotubes

Xin Chang, Sapanbir S. Thind, and Aicheng Chen*

Department of Chemistry, Lakehead University, 955 Oliver Road, Thunder Bay, Ontario P7B 5E1, Canada

ABSTRACT: In this study, TiO_2 nanotubes were treated via electrochemical reduction and tested as a novel catalyst, for the first time, toward the electrochemical oxidation of salicylic acid (SA), where the effects of cathodic current and reduction time were systemically investigated. The fabricated TiO_2 nanotubes were characterized using scanning electron microscopy (SEM), X-ray diffraction (XRD), and X-ray photoelectron spectroscopy (XPS). Cyclic voltammetry (CV), chronoamperometry, chronopotentiometry, ultraviolet−visible light (UV-vis) absorbance spectroscopy, and Mott−Schottky plots were employed to study the enhanced electrochemical activity of the TiO_2 nanotubes. Our experimental results revealed that the optimal electrochemical treatment conditions were −5 mA cm^{-2} for 10 min. The treated TiO_2 nanotubes possessed a much higher overpotential for oxygen evolution than a Pt electrode, and exhibited a high electrocatalytic activity toward the oxidation of SA. The oxidation of SA at the treated TiO_2 nanotubes was shown to be 6.3 times greater than a Pt electrode. Stability tests indicated that treated TiO_2 nanotubes are very stable over eight cycles of electrochemical oxidation of SA. The high electrocatalytic activity and stability of the treated TiO_2 nanotubes enabled by the facile electrochemical reduction can be attributed to the decrease of Ti(IV), the increase of Ti(II) and Ti(III), and the increase of the oxygen vacancies, as well as significant improvement of the donor density.

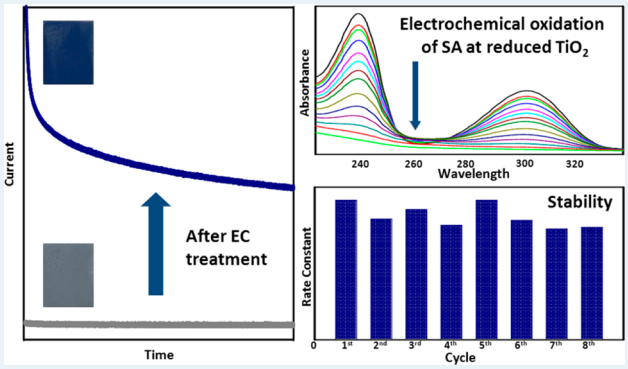

KEYWORDS: *electrocatalysis, TiO_2 nanotubes, electrochemical treatment, salicylic acid, donor density, overpotential of oxygen evolution*

1. INTRODUCTION

TiO_2 is undeniably one of the most intensely studied semiconductors in materials science, because of its unique combination outstanding properties, such as biological and chemical inertness, high efficiency, low cost, environmental tolerance, and high stability.[1−4] Despite significant efforts that have been expended toward the application of TiO_2 as a photocatalyst,[5] its photochemical utility has been impeded by the fact that it may only be activated by UV light, because of its large bandgap (~3.0 eV for rutile and ~3.2 eV for anatase).[6−8] As a consequence, great interest has arisen in the performance of bandgap engineering (e.g., narrowing of the bandgap) and a myriad of techniques have been applied toward enabling TiO_2, to thus efficiently utilize solar energy. These approaches encompass doping with nonmetal elements, reduction via the application of vacuum or reducing conditions (e.g., H_2), chemical vapor deposition, and high-energy particle bombardment.[9−16]

Salicylic acid (SA) is a common organic water pollutant that is generated by the cosmetics industry, pharmaceutical wastewater, paper mill wastewater, and landfill leachate.[17−20] It is known, for example, that salicylic acid has an ototoxic effect and can also bring about salicylism, fetal abnormalities, and central nervous system depression damage.[21,22] Therefore, a heightened interest in the investigation of advanced technologies to treat SA has evolved, driven by the inefficiencies of conventional treatment processes. Recent studies have indicated that advanced oxidation processes (AOPs), especially electrochemical methods, are very attractive for the treatment of water that has been contaminated with organic substances.[23−30] In contrast with other technologies (e.g., wet air oxidation processes (WAO)) that require severe operational conditions,[31,32] the removal of pollutants utilizing electrochemical methods may be achieved at room temperature under ambient atmospheric pressure. A wide variety of anode materials have been reported to facilitate the electrochemical remediation of organic compounds, including carbon, Pt, PbO_2, IrO_2, SnO_2, Pt−Ir, and boron-doped diamond (BDD) electrodes.[33−38] Although these catalysts are widely employed due to their high electric conductivity, they also harbor a number of weak points such as toxicity, high energy consumption, and expense. Since the discovery of the photocatalytic oxidation of water over TiO_2, minimal research has been conducted in the study of TiO_2 as an electrocatalyst,

Received: April 14, 2014
Revised: June 21, 2014
Published: June 27, 2014

because its low electrical conductivity prevents its use as such. There exist a few reports in the literature that describe the modification of TiO_2 with carbon or noble metals with the objective of increasing its conductivity and subsequent use for the electrochemical reduction of organic pollutants. To the best of our knowledge, no work has been reported that utilizes electrochemically reduced TiO_2 as an electrocatalyst for the electrochemical oxidation of SA in wastewater treatment.

In the present work, we report on the discovery of the significantly enhanced electrochemical activity of TiO_2 nanotubes that were treated by electrochemical reduction and tested as a novel electrocatalyst for the electrochemical oxidation of SA. Scanning electron microscopy (SEM), X-ray diffraction (XRD), X-ray photoelectron spectroscopy (XPS), cyclic voltammetry (CV), chronamperometry, and chronopotentiometry were employed to characterize the structure, morphology, composition, and electrochemical activity of the TiO_2 nanotubes. The effects of time and current on the electrochemical reduction process were investigated to elucidate optimal treatment conditions. Moreover, the electrocatalytic behavior of the reduced TiO_2 was studied using the electrochemical oxidation of 30 ppm of SA in 0.1 M H_2SO_4 under a 3 mA cm^{-2} applied current at room temperature. The oxidation of SA at treated TiO_2 nanotubes was found to be 6.3 times greater than that at a Pt electrode. In addition, the stability and donor density of the TiO_2 nanotubes were also studied.

2. EXPERIMENTAL SECTION

2.1. Materials. Reagent-grade salicylic acid (99+%) and titanium plates (99.2%) were purchased from Sigma−Aldrich and Alfa Aesar, respectively, and used as received. All other utilized chemicals were of reagent grade and used as supplied. The water (18.2 MΩ cm) that was utilized for all experimental solutions was purified by a Nanopure Diamond water system.

2.2. Fabrication and Treatment of TiO_2 Nanotubes. The TiO_2 nanotubes were grown directly on titanium plates (1.25 cm × 0.8 cm × 0.5 mm) utilizing anodic oxidation. The Ti plates were initially sonicated in acetone, rinsed with pure water, and then etched in 18% HCl at 85 °C for 10 min. The etched titanium plate was then submerged in a one-compartment, two-electrode cell, containing DMSO + 2% HF, and was electrochemically treated at 40 V for 7 h. To ensure that the anatase crystal structure of the TiO_2 was obtained, the plates were annealed at 450 °C for 3 h. The TiO_2 nanotubes were then treated in 0.1 M H_2SO_4 at different cathodic current densities varied from −2.5 mA cm^{-2} to −10 mA cm^{-2} for a different period of time varied from 2.5 min to 40 min.

2.3. Characterization of the Synthesized TiO_2 Nanotubes. The synthesized TiO_2 nanotubes were characterized by SEM (JEOL, Model 5900LV) and XRD (Philips, Model PW 1050-3710 diffractometer with Cu Kα radiation). The surface composition was examined by XPS (Omicron EA-125 energy analyzer and a multichannel detector). All binding energies reported in this work were corrected using the C 1*s* peak at 284.5 eV as an internal standard. The broad Ti 2p region of the sample was fitted using XPSPEAK41 software. A three-electrode cell system was employed for the electrochemical studies. A Pt coil with a 10 cm^2 surface area was utilized as the auxiliary electrode, and a Ag/AgCl electrode was used as the reference electrode. To enable a comparison to the TiO_2 working electrodes, a 1 cm^2 polycrystalline Pt wire was also employed as the working electrode. The current density was calculated based on the geometric surface area. The electrochemical measurements were carried out at room temperature (20 ± 2 °C) using a Voltalab 40 Potentiostep (PGZ301). CV, chronoamperometry, and chronopotentiometry were used to characterize the electrochemical activity of TiO_2 nanotubes. Cyclic voltammograms (CVs) were recorded in a 0.1 M H_2SO_4 solution at a sweep rate of 20 mV/s, whereas chronoamperometric curves were measured where the electrode potential was held at 0 V for 30 s and then increased to 2.4 V for 5 min. Mott−Schottky plots were measured at a fixed frequency of 500 Hz in a 0.1 M H_2SO_4 solution.

2.4. Electrochemical Oxidation of Salicylic Acid in 0.1 M H_2SO_4. The synthesized TiO_2 nanotubes were utilized as the working electrode; a Pt coil served as the counter electrode, whereas the reference electrode was comprised of Ag/AgCl. The UV/vis spectra of SA were recorded over the range of 200−450 nm in order to monitor the oxidation process in situ, using a Cary 50 UV/vis spectrophotometer, displaying two peaks at ca. 236 and 302 nm, respectively. The peak at 236 nm was employed as the calibration curve due to the relatively high sensitivity.

A seven-point calibration was conducted with SA concentrations that varied from 0 to 30 ppm. A linear relationship was achieved with the regression equation

$$C\ (\text{ppm}) = 16.40A - 0.1102$$

(figure not shown). Good correlation coefficients ($R^2 = 0.999$) indicated that the 236-nm peak could be used to adequately convert absorbance readings to concentrations.

3. RESULTS AND DISCUSSION

3.1. Characterization of TiO_2 Nanotubes. The structure and morphology of the TiO_2 nanotubes were characterized by SEM. As shown in Figure 1A, the synthesized self-organized nanotubes consisted of pored arrays with uniform diameters of ca. 100 nm where the pore lumens were open at the top of the layer. The EDX of the nanotubes (Figure 1B) illustrated strong O and Ti peaks, which confirmed the composition of the formed nanotube arrays. Figure 1C revealed the corresponding XRD patterns of the prepared TiO_2 nanotubes prior to and following the electrochemical reduction. Except for the peaks (marked with stars), derived from the Ti substrate, all of the diffraction peaks were attributed to the tetragonal anatase TiO_2, showing that the formed TiO_2 nanotubes exist in the anatase phase. Moreover, the XRD spectra prior to and following the electrochemical reduction were almost identical, indicating that there was no alteration in the crystalline structure subsequent to the electrochemical reduction.

3.2. Electrochemical Reduction of TiO_2 Nanotubes. In order to elucidate the optimal electrochemical reduction conditions, the effects of applied current and time on the electrochemical activity of the TiO_2 nanotubes were examined with different applied current densities, spanning −2.5, −5, −7.5, and −10 mA cm^{-2} over different timelines, respectively. The second cycles of the CVs of the TiO_2 nanotubes prior to and following electrochemical reductions, which employed different current densities, are depicted in Figure 2A and 2B, respectively. The shape of the CVs and the corresponding currents remained constant with the subsequent cycling. The CV results of four electrodes (#1−#4) of the TiO_2 nanotube prior to electrochemical reduction are very similar, and they may be divided into two distinct regions: (I) the region at an initial stage where hydrogen adsorption/desorption proceeds between −0.2 V and 0.35 V; and (II) the double-layer charging

dx.doi.org/10.1021/cs500487a | ACS Catal. 2014, 4, 2616−2622

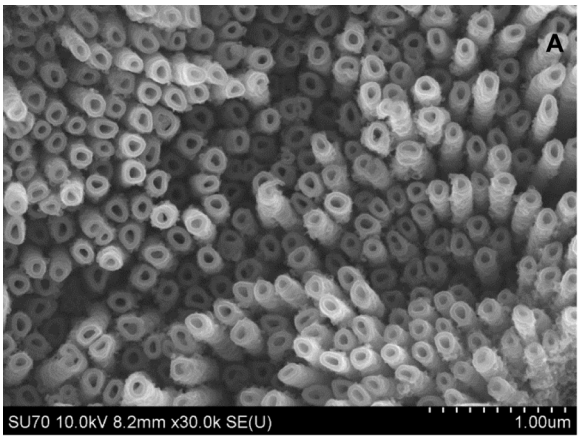

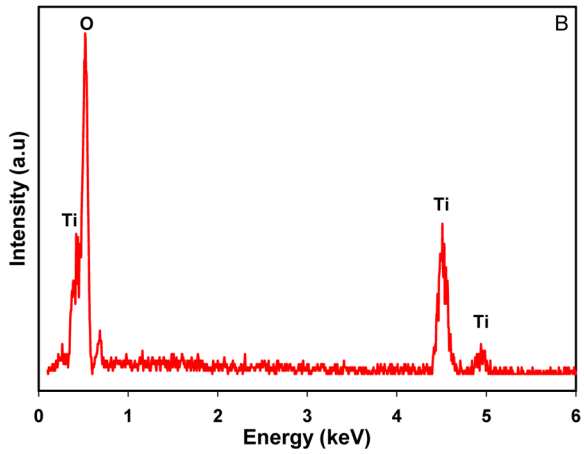

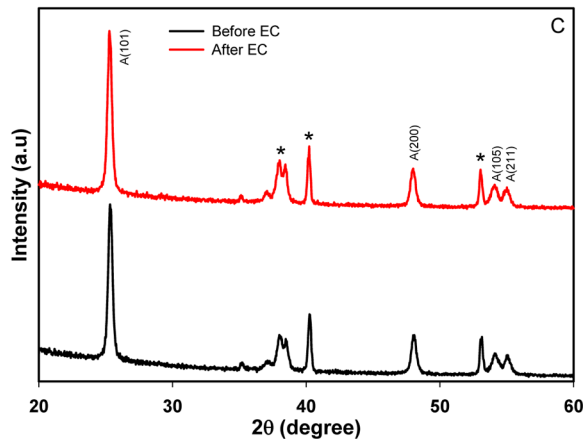

Figure 1. (A) SEM image, (B) EDX spectrum, and (C) XRD spectra of the fabricated TiO_2 nanotubes.

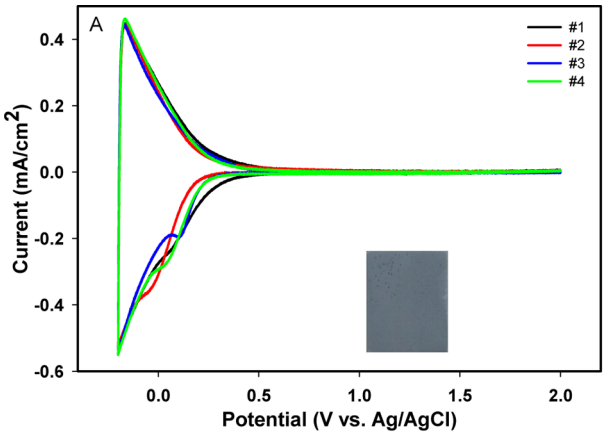

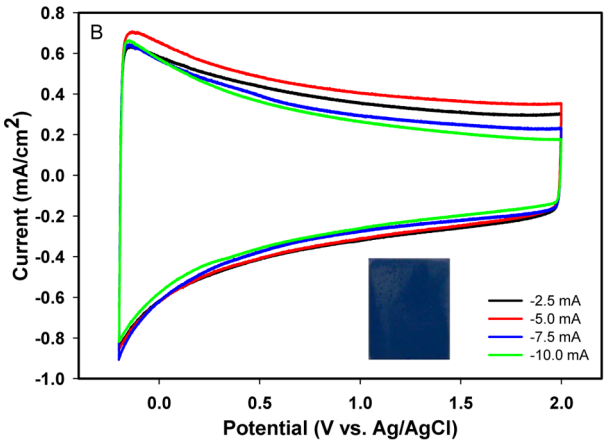

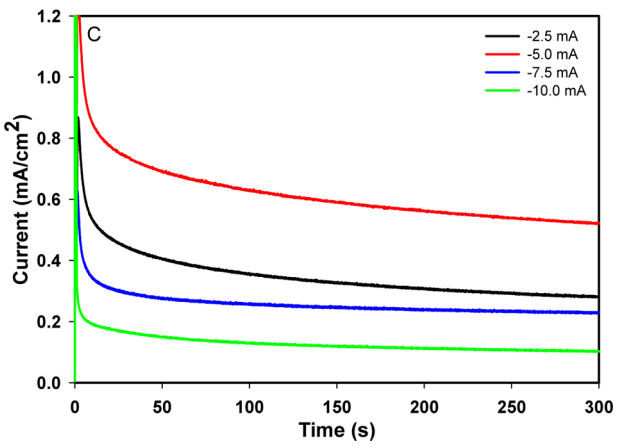

Figure 2. Cyclic voltammograms of the TiO_2 nanotube electrodes (A) prior to and (B) following the treatment at different currents for 10 min in 0.1 M H_2SO_4 at a sweep rate of 20 mV/s. (C) Chronoamperometric curves of the TiO_2 nanotube electrodes treated at different currents for 10 min in 0.1 M H_2SO_4. Insets in panels A and B are digital images of the TiO_2 nanotubes prior to and following electrochemical reduction.

region, between 0.35 V and 2.0 V. As shown in Figure 2B, the current was significantly increased, following the electrochemical reduction with various applied current densities varied from -2.5 mA cm^{-2} to -10 mA cm^{-2}, especially in Region II. An almost rectangular CV curve was observed, showing that the electrochemically treated TiO_2 nanotubes behaved as a pure capacitor. Meanwhile, the color of the TiO_2 nanotube electrode was dramatically affected by the electrochemical reduction process. As can be seen in the insets of Figure 2A and 2B, the original gray color of the electrode was transitioned to dark blue, indicative of structural changes in the TiO_2 that were initiated by the treatment. Figure 2C presents the chronoamperometric curves of the TiO_2 nanotubes that were treated under different current densities for 10 min, showing that the achieved steady-state current densities of the treated TiO_2 nanotubes strongly depend on the applied cathodic current densities. The cathodic tratement under -5.0 mA cm^{-2} resulted in the highest steady-state current.

dx.doi.org/10.1021/cs500487a | ACS Catal. 2014, 4, 2616−2622

To optimize the cathodic treatment conditions, we further investigated the effect of time on the electrochemical reduction of the TiO_2 nanotubes at −5.0 mA cm^{-2}. Figure 3 presents the CVs and chronoamperometric curves of the TiO_2 nanotubes before and after the cathodic treatment over different time intervals. As shown in Figure 3A, even being reduced for only 2.5 min, the CV was dramatically changed in comparison with the initial CV. However, no obvious changes were observed when the reduction time was increased from 2.5 min to 40 min. In contrast, significant differences were seen in the chronoamperometric curves presented in Figure 3B. Figure 3C displays the steady-state current densities which were measured from the chronoamperometric curves at 300 s, showing that 10 min was optimal in maintaining the highest current density, which is ∼30 times higher than that of the untreated TiO_2 nanotube electrode. Higher current or longer time may decrease the stability of the TiO_2 nanotubes or even results in detaching the TiO_2 nanotubes from the Ti substrate.

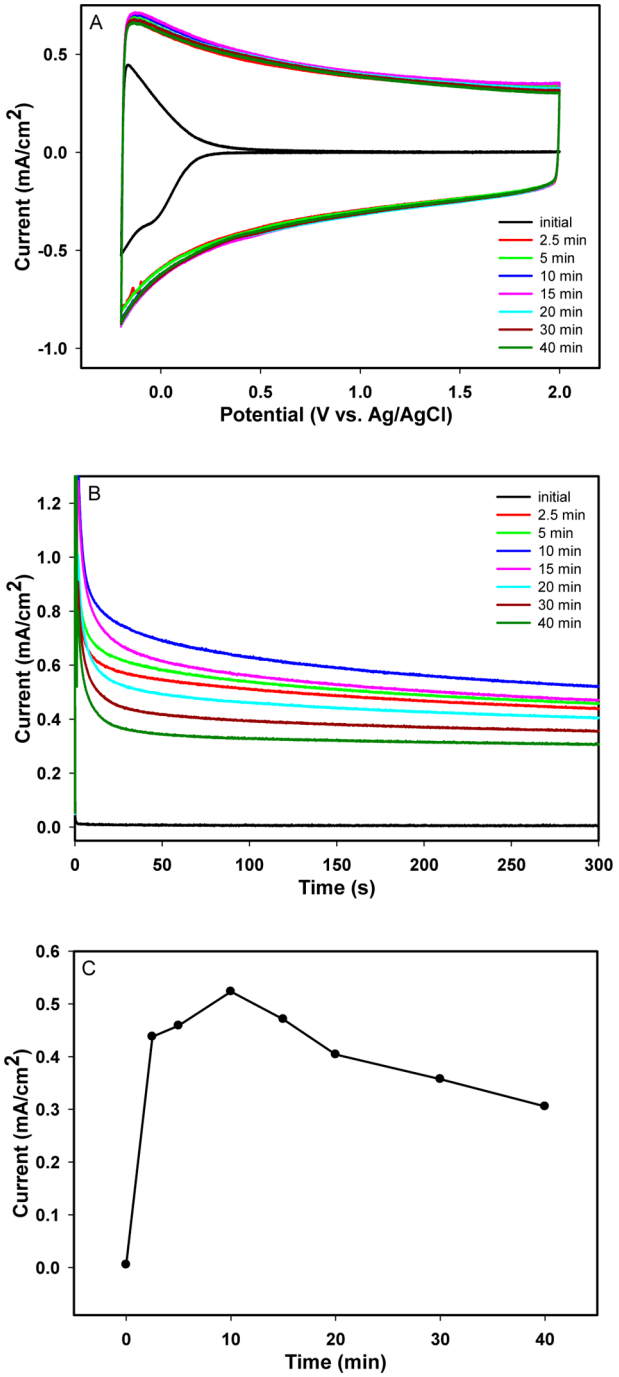

Figure 3. (A) Cyclic voltammograms and (B) chronoamperometric curves of the TiO_2 nanotube electrode before and after being cathodically treated at −5 mA cm^{-2} for different time periods in 0.1 M H_2SO_4 at 2.4 V. (C) Plot of the steady-state currents measured at 300 s from the curves presented in panel B versus the time of the electrochemical treatment.

3.3. Electrochemical Oxidation of SA at the Treated TiO_2 Nanotube Electrode. For comparison, a polycrystalline Pt electrode with a geometric surface area of 1 cm^2 was also tested in this study. The CVs of the treated TiO_2 nanotubes cathodically treated under the optimal conditions (−5.0 mA cm^{-2} and 10 min) and the Pt electrode, recorded in 30 ppm of SA in a 0.1 M H_2SO_4 solution, are presented in Figure 4A,

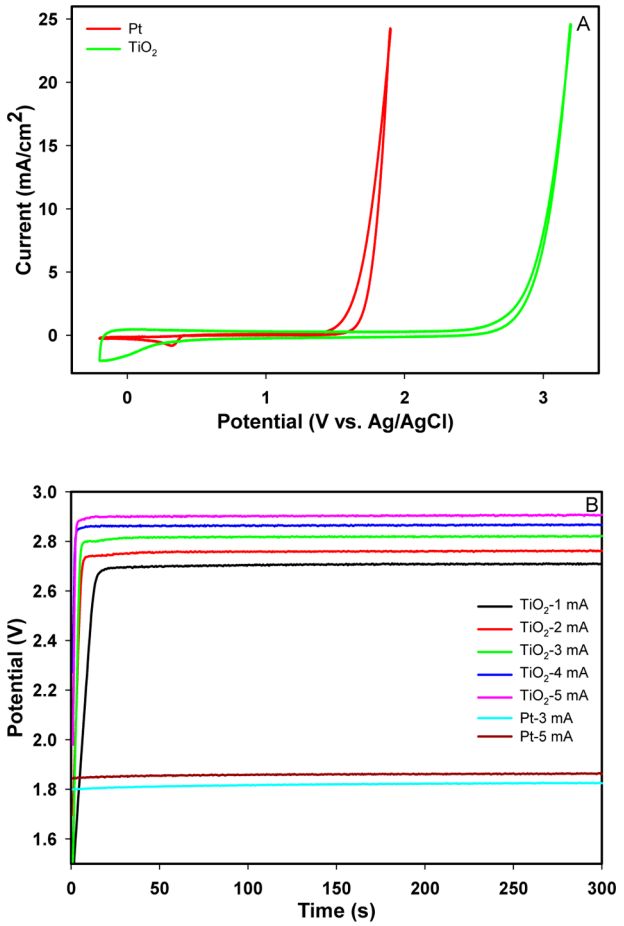

Figure 4. Comparison of the cyclic voltammograms (A) and chronopotentiometric curves (B) of the treated TiO_2 nanotubes and a Pt electrode recorded in 0.1 M H_2SO_4 + 30 ppm of SA.

showing that the overpotential for oxygen evolution was dramatically increased from ∼1.3 V for the Pt electrode to ∼2.6 V for the treated TiO_2 nanotubes. It is interesting to note that the CV curve of the treated TiO_2 nanotubes recorded in the absence of SA was almost identical to the CV curve measured in the presence of SA, as shown in Figure 4A, indicating that direct electrochemical oxidation of SA occurred due to the generation of •OH at the TiO_2 nanotubes. The significant potential increase was further evidenced by the chronopoten-

dx.doi.org/10.1021/cs500487a | ACS Catal. 2014, 4, 2616−2622

tiometric (CP) measurements presented in Figure 4B. It is well-known that the high overpotentail for oxygen evolution is highly beneficial to the electrochemical oxidation of organic pollutants. Lead dioxide and BDD electrodes have been widely studied as anode materials for electrochemical treatment of wastewater, because of their inherent high overpotential for oxygen evolution.[39] All the aforementioned results suggest that the treated TiO_2 nanotubes can be classified as an "inactive" electrode, like BDD, and would be more optimal for applications in the electrochemical oxidation of organic pollutants than the Pt electrode.

In order to determine the enhanced activity of electrochemically treated TiO_2 nanotube electrode, we investigated the electrochemical oxidation of SA at different applied current densities. Figure 5A presents the time dependence of the spectra absorbance of 30 ppm of SA in 0.1 M H_2SO_4 with an applied current of 3 mA cm^{-2} during the electrochemical oxidation at the treated TiO_2 nanotubes. The UV-vis spectra were taken every 5 min for the initial 10 min, then every 10 min for the remaining 50 min and every 20 min for the final 2 h. The absorbance peaks of SA at 236 (peak a) and 303 nm (peak b) decreased with the increase of the electrochemical oxidation time. Peak a approached 0.197 after 3 h of degradation, corresponding to ca. 90% removal of SA from the solution. For comparison, the electrochemical oxidation of SA was also performed at a Pt polycrystalline electrode under the same experimental condition (Figure 5B), where ~21% removal of SA from solution was observed.

Based on the linear regression equation developed in section 2.4 and the absorbance peak at 236 nm, we calculated the concentrations of SA during electrochemical oxidation. As shown in Figure 5C, the electrochemical oxidation of SA at treated TiO_2 nanotubes and Pt wires was fitted well, based on the first-order kinetics. The derived rate constants are listed in Table 1. It was increased from 9.22×10^{-3} min^{-1} to 1.06×10^{-2} min^{-1} with an increase of the applied current density from 2.0 mA cm^{-2} to 3.0 mA cm^{-2}, showing that higher applied currents had a positive effect on the oxidation of SA at the treated TiO_2 nanotubes. However, the rate constant was only slightly increased with further increases in the current density from 3.0 mA cm^{-2} to 4.0 and 5.0 mA cm^{-2}. In cognizance of power consumption, 3.0 mA cm^{-2} was selected as the optimized current for the electrochemical oxidation of SA at the treated TiO_2 nanotubes. It is interesting to note that the rate constant for the oxidation of SA at the treated TiO_2 nanotubes is more than six times higher than that at the Pt electrode at the applied current density of 3.0 mA cm^{-2}. Comparison of the UV−visible spectra displayed in Figure 5A and Figure 5B indicates that the mechanisms of the SA oxidation are different. Complete oxidation of SA occurred on the treated TiO_2 nanotubes, because of the generation of •OH, whereas partial oxidation was observed on the Pt electrode. All these results further show that the high overpotential of oxygen evolution is beneficial toward the electrochemical oxidation of organic pollutants.

3.4. Electrochemical Stability of the Treated TiO_2 Nanotubes. To further examine the electrocatalytic stability of the electrochemically reduced TiO_2 nanotubes, eight cycles of the electrochemical oxidation of 30 ppm of SA in a 0.1 M H_2SO_4 solution were carried out. The applied current density was 3.0 mA cm^{-2} and the oxidation duration was 3 h. Figure 6 presents the change of the SA concentration versus time for each run, which were further fitted using the first-order kinetics.

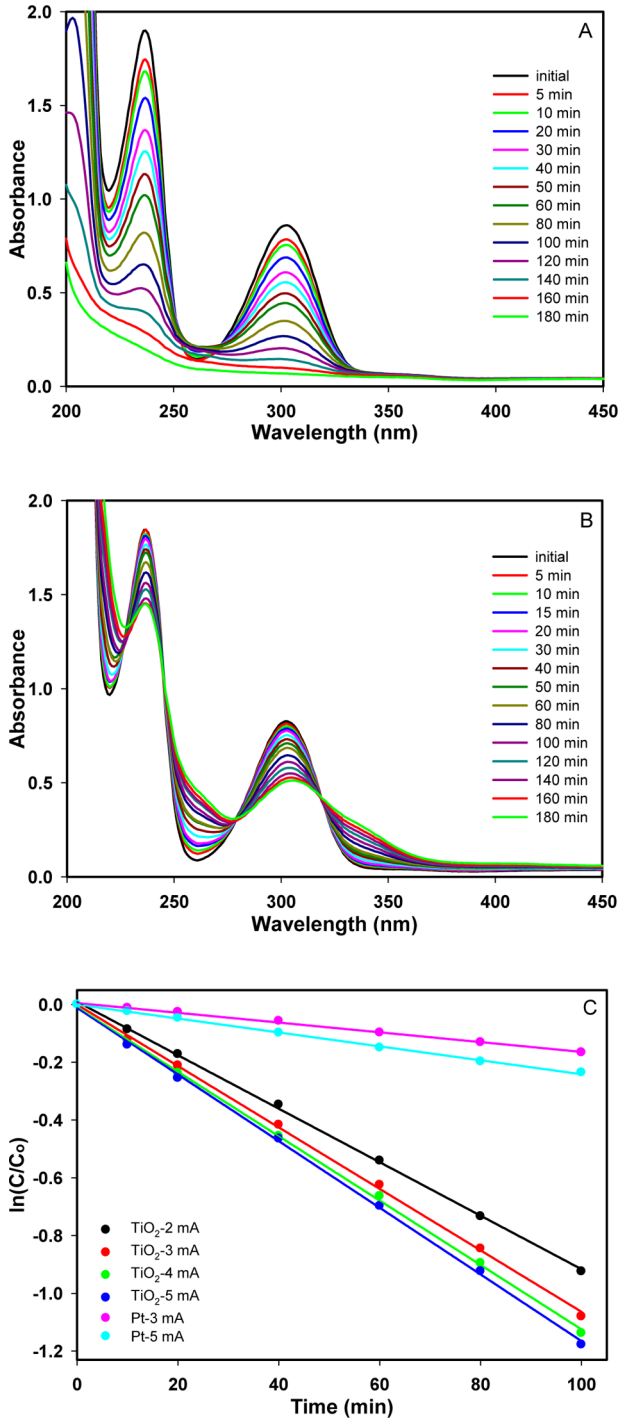

Figure 5. Absorbance spectra for the electrochemical oxidation of 30 ppm of SA in 0.1 M H_2SO_4 at (A) the treated TiO_2 nanotubes and (B) the Pt electrode with a current density of 3 mA cm^{-2}. (C) Plot of $\ln(C/C_0)$ versus time of the electrochemical oxidation of SA at the treated TiO_2 nanotubes and the Pt electrode with different current densities.

The relative standard deviation obtained from the quantitative analysis of kinetic curves was only ca. 1%, which was indicative of the remarkable stability of the electrochemically treated TiO_2 nanotubes.

3.5. XPS Analysis and Mott−Schottky Study. To elucidate the high catalytic activity and stability of the TiO_2 nanotubes enabled by the cathodically treatment, XPS was

dx.doi.org/10.1021/cs500487a | ACS Catal. 2014, 4, 2616−2622

Table 1. First-Order Kinetic Constants and Relative Coefficients for the Electrochemical Oxidation of SA at the TiO_2 Nanotubes Treated at −5 mA cm^{-2} for 10 min and a Pt Electrode

electrode	current density (mA cm^{-2})	rate constant (min^{-1})	R^2
TiO_2 nanotubes	2.0	9.22×10^{-3}	0.999
TiO_2 nanotubes	3.0	1.06×10^{-2}	0.999
TiO_2 nanotubes	4.0	1.11×10^{-2}	0.999
TiO_2 nanotubes	5.0	1.15×10^{-2}	0.999
Pt	3.0	1.69×10^{-3}	0.997
Pt	5.0	2.40×10^{-3}	0.998

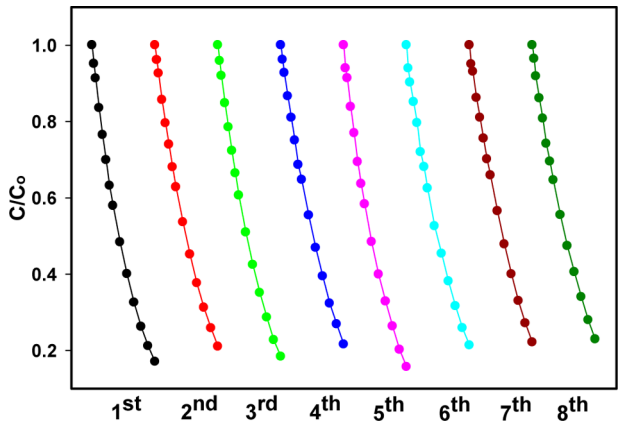

Figure 6. Stability tests of the treated TiO_2 nanotubes. Plots of C/C_0 versus time of electrochemical oxidation of 30 ppm of SA at the applied current density of 3 mA cm^{-2}.

employed to characterize the change of chemical compositions and electronic states of the TiO_2 nanotube electrodes before and after the electrochemical reduction. The XPS survey scan of the TiO_2 nanotubes is presented in Figure 7A, showing that the Ti 2p core level was at 458.78 eV, the O 1s core level was at 530.06 eV, while the C 1s core level was at 284.58 eV, which further confirmed the composition of the formed nanotube arrays. The high-resolution XPS spectrum of TiO_2 nanotubes after being treated in 0.1 M H_2SO_4 with −5 mA cm^2 for 10 min is shown in Figure 7B. It reveals that the peaks for Ti^{4+}, Ti^{3+}, and Ti^{2+} were centered at 459.11, 457.90, and 456.81 eV, respectively. This clearly illustrated the presence of different Ti oxidation states within the sample. The atomic percentages of different oxidation states of Ti and O were calculated from XPS prior to and following electrochemical reduction. The level of Ti(IV) decreased from 93.86% to 92.13% subsequent to reduction, while Ti(III) and Ti(II) increased, following the reduction, from 3.81% to 4.61% and 2.33% to 3.25%, respectively. This revealed that a portion of the Ti(IV) was transformed to Ti(III) and Ti(II) during the electrochemical reduction process. In addition, the level of O(II) decreased from 86.39% to 78.97% after the 10-min reduction, indicating an increase of oxygen vacancies, which may further enhance the electrochemical activity of the treated TiO_2 nanotubes.

To further characterize the change of the electronic properties of the TiO_2 nanotubes prior to and following the electrochemical reduction, Mott−Schottky measurements were carried out in a 0.1 M H_2SO_4 solution.[40,41] Figure 8 presents the Mott−Schottky plots of the as-synthesized TiO_2 nanotubes and electrochemically treated TiO_2 nanotubes. A sigmoidal plot

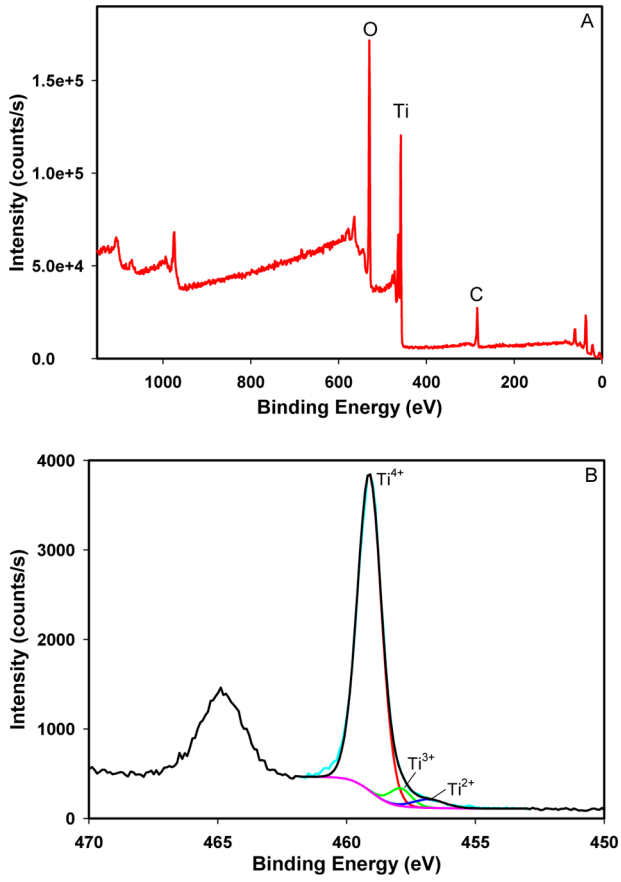

Figure 7. (A) XPS survey scan spectrum of as-prepared TiO_2 nanotubes and (B) a high-resolution XPS spectrum of Ti of the TiO_2 nanotubes after being treated at −5 mA cm^{-2} for 10 min.

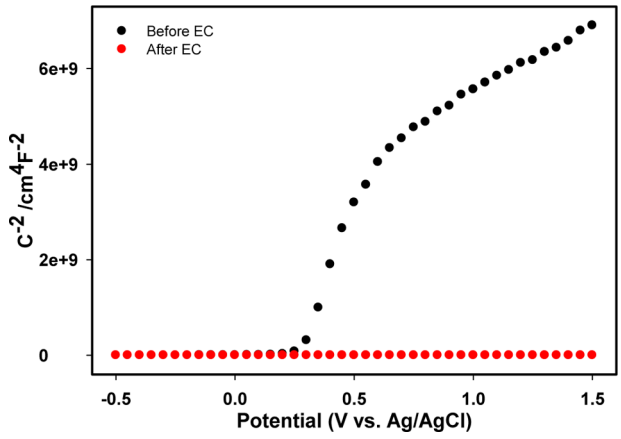

Figure 8. Mott−Schotty plots of the TiO_2 nanotubes obtained in 0.1 M H_2SO_4 at 500 Hz prior to and following the electrochemical reduction.

was observed in the investigated potential range, which was typical for *n*-type semiconductors. There was a good linear relationship between C^{2-} and the potential in the range of 0.3 and 0.6 V for the nontreated TiO_2 nanotubes, as well as the electrochemically treated TiO_2 nanotubes. It is intriguing to note that the donor density of the electrochemically treated TiO_2 nanotubes was estimated from the Mott−Schottky relationship to be 3.1×10^{22} cm^{-3}, which is more than 33 000 times larger than that of the untreated TiO_2 nanotubes (9.3

dx.doi.org/10.1021/cs500487a | ACS Catal. 2014, 4, 2616−2622

$\times 10^{17}$ cm^{-3}), showing that the electrochemical treatment significantly increased the conductivity of the TiO_2 nanotubes.

4. CONCLUSIONS

In summary, we have demonstrated a facile and effective approach for the significant enhancement of the electrocatalytic activity of the TiO_2 nanotubes. For the first time, TiO_2 nanotubes were treated via electrochemical reduction and tested as a novel catalyst for the electrochemical oxidation of salicylic acid (SA). Optimal reduction conditions were investigated, which revealed that an applied current of −5 mA cm^{-2} under 10 min of electrochemical reduction gave the best results. The reduced TiO_2 nanotubes possessed a much higher overpotential for oxygen evolution than a Pt electrode and exhibited a high electrocatalytic activity toward the oxidation of SA. Using a 30 ppm of SA solution, ca. 90% of SA was electrochemically oxidized over 3 h at 3.0 mA cm^{-2}; and under the identical operational conditions, an only ca. 21% removal of SA was observed at a Pt polycrystalline electrode. The rate constant for the electrochemical oxidation of SA at the reduced TiO_2 nanotubes was determined to be 1.06×10^{-2} min^{-1}, which is over six times higher than that at the Pt electrode. The high electrocatalytic activity and stability of the TiO_2 nanotubes enabled by the facile electrochemical reduction can be attributed to (i) the decrease of Ti(IV); (ii) the increase of Ti(II) and Ti(III); (iii) the increase of the oxygen vacancies; and (iv) the significant improvement of the donor density. The cathodically treated TiO_2 nanotubes possess a similar overpotential for oxygen evolution as the boron-doped diamond electrode, one of the highest performance electrode materials for the electrochemical oxidation of organic pollutants, but with a significant lower cost. Thus, the facile approach described in this study open a door for the development of high-performance electrode materials for electrochemical treatment of wastewater and green chemistry applications.

AUTHOR INFORMATION

Corresponding Author

*Fax: 1-807-346-7775. E-mail: achen@lakeheadu.ca.

Notes

The authors declare no competing financial interest.

ACKNOWLEDGMENTS

This work was supported by a Discovery Grant from the Natural Sciences and Engineering Research Council of Canada (NSERC). A.C. acknowledges the NSERC and the Canada Foundation for Innovation (CFI) for the Canada Research Chair Award in Materials & Environmental Chemistry.

REFERENCES

(1) Tian, M.; Wu, G.; Chen, A. *ACS Catal.* **2012**, *2*, 425−432.
(2) Wu, G.; Nishikawa, T.; Ohtani, B.; Chen, A. *Chem. Mater.* **2007**, *19*, 4530−4537.
(3) Yu, Y.; Ren, J.; Liu, D.; Meng, M. *ACS Catal.* **2014**, *4*, 934−941.
(4) Luan, Y.; Jing, L.; Xie, Y.; Sun, X.; Feng, Y.; Fu, H. *ACS Catal.* **2013**, *3*, 1378−1385.
(5) Muñoz-Batista, M.; Gómez-Cerezo, M.; Kubacka, A.; Tudela, D.; Fernández-García, M. *ACS Catal.* **2014**, *4*, 63−72.
(6) Lee, W. J.; Lee, J. M.; Kochuveedu, S. T.; Han, T. H.; Jeong, H. Y.; Park, M.; Yun, J. M.; Kwon, J.; No, K.; Kim, D. H.; Kim, S. O. *ACS Nano* **2012**, *6*, 935−943.
(7) Chen, X. B.; Mao, S. S. *Chem. Rev.* **2007**, *107*, 2891−2959.
(8) Hwang, Y. J.; Hahn, C.; Liu, B.; Yang, P. *ACS Nano* **2012**, *6*, 5060−5069.
(9) Shiraishi, Y.; Fujiwara, K.; Sugano, Y.; Ichikawa, S.; Hirai, T. *ACS Catal.* **2013**, *3*, 312−320.
(10) Hashimoto, K.; Masuda, Y.; Kominami, H. *ACS Catal.* **2013**, *3*, 1349−1355.
(11) Li, K.; Chai, B.; Peng, T.; Mao, J.; Zan, L. *ACS Catal.* **2013**, *3*, 170−177.
(12) Thind, S. S.; Wu, G.; Chen, A. *Appl. Catal., B* **2012**, *111*, 38−45.
(13) Shi, J.; Wang, X. D. *Energy Environ. Sci.* **2012**, *5*, 7918−7922.
(14) Thind, S. S.; Wu, G.; Tian, M.; Chen, A. *Nanotechnology* **2012**, *23*, 475706.
(15) Thompson, T. L.; Yates, J. T. *Chem. Rev.* **2006**, *106*, 4428−4453.
(16) Zuo, F.; Wang, L.; Wu, T.; Zhang, Z. Y.; Borchardt, D.; Feng, P. Y. *J. Am. Chem. Soc.* **2010**, *132*, 11856−11857.
(17) Adán, C.; Coronado, J. M.; Bellod, R.; Soria, J.; Yamaoka, H. *Appl. Catal., A* **2006**, *303*, 199−206.
(18) Vilambi, N. R. K.; Chin, D. T. *J. Electrochem. Soc.* **1987**, *134*, 3074−3077.
(19) Mills, A.; Holland, C. E.; Davies, R. H.; Worsley, D. *J. Photochem. Photobiol., A* **1994**, *83*, 257−263.
(20) Carlotti, M. E.; Sapino, S.; Trotta, M.; Vione, D.; Minero, C.; Peira, E. *J. Dispersion Sci. Technol.* **2007**, *28*, 805−818.
(21) Matyasovszky, N.; Tian, M.; Chen, A. *J. Phys. Chem. A* **2009**, *113*, 9348−9353.
(22) Goi, A.; Veressinina, Y.; Trapido, M. *Chem. Eng. J.* **2008**, *143*, 1−9.
(23) Quiroz, M. A.; Reyna, S.; Martinez-Huitle, C. A.; Ferro, S.; DeBattisti, A. *Appl. Catal., B* **2005**, *59*, 259−266.
(24) Tian, M.; Bakovic, L.; Chen, A. *Electrochim. Acta* **2007**, *52*, 6517−6524.
(25) Borras, C.; Laredo, T.; Scharifker, B. R. *Electrochim. Acta* **2003**, *48*, 2775−2780.
(26) Vinodgopal, K.; Hotchandani, S.; Kamat, P. V. *J. Phys. Chem.* **1993**, *97*, 9040−9044.
(27) Leng, W. H.; Zhu, W. C.; Ni, J.; Zhang, Z.; Zhang, J. Q.; Cao, C. N. *Appl. Catal., A* **2006**, *300*, 24−35.
(28) Li, J.; Zhang, X.; Ai, Z.; Jia, F.; Zhang, L.; Lin, J. *J. Phys. Chem. C* **2007**, *111*, 6832−6836.
(29) Tian, M.; Wu, G. S.; Adams, B.; Wen, J. L.; Chen, A. *J. Phys. Chem. C* **2008**, *112*, 825−831.
(30) Yun, H. J.; Lee, H.; Joo, J. B.; Kim, W.; Yi, J. *J. Phys. Chem. C* **2009**, *113*, 3050−3055.
(31) Yadav, B. R.; Garg, A. *Ind. Eng. Chem. Res.* **2012**, *51*, 15778−15785.
(32) Lefevre, S.; Ferrasse, J.; Faucherand, R.; Viand, A.; Boutin, O. *Energy.* **2012**, *41*, 175−183.
(33) Tian, M.; Adams, B.; Wen, J.; Asmussen, R. M.; Chen, A. *Electrochim. Acta* **2009**, *54*, 3799−3805.
(34) Martinez-Huitle, C. A.; Ferro, S. *Chem. Soc. Rev.* **2006**, *35*, 1324−1340.
(35) Comninellis, C. *Electrochim. Acta* **1994**, *39*, 1857−1862.
(36) Canizares, P.; Lobato, J.; Paz, R.; Rodrigo, M. A.; Sáez, C. *Water Res.* **2005**, *39*, 2687−2703.
(37) Zhao, X.; Liu, H.; Qu, J. *Catal. Commun.* **2010**, *12*, 76−79.
(38) Rodgers, J. D.; Bunce, N. J. *Environ. Sci. Technol.* **2001**, *35*, 406−410.
(39) Pan, K.; Tian, M.; Jiang, Z.-H.; Kjartanson, B.; Chen, A. *Electrochim. Acta* **2012**, *60*, 147−153.
(40) Munoz, A. G. *Electrochim. Acta* **2007**, *52*, 4167−4176.
(41) Gimenez, S.; Dunn, H. K.; Rodenas, P.; Fabregat-Santiago, F.; Miralles, S. G.; Barea, E. M.; Trevisan, R.; Guerrero, A.; Bisquert, J.; Gimenez, S. *J. Electroanal. Chem.* **2012**, *668*, 119−125.